# Continuous subsidence associated to the long lasting eruption of Arenal volcano (Costa Rica) observed by dry tilt stations

Mauricio M. Mora, Philippe Lesage, Fabien Albino, Gerardo Soto, Guillermo E. Alvarado

# *Continuous subsidence associated to the long lasting eruption of Arenal volcano (Costa Rica) observed by dry tilt stations*

**Mauricio M. Mora[1+], Philippe Lesage[2], Fabien Albino[2], Gerardo J. Soto[3,4] and Guillermo E. Alvarado[3]**

[1]*Escuela Centroamericana de Geología, Universidad de Costa Rica, Apdo. 214-2060, Costa Rica. Corresponding author: e-mail address: mmmora@geologia.ucr.ac.cr; tel. +506-2253-8407; fax +506-2253-2586.*

[2]*Laboratoire de Géophysique Interne et Tectonophysique, CNRS, Université de Savoie, 73376 Le Bourget-du-Lac Cedex, France.*

[3]*Área de Amenazas y Auscultación Sísmica y Volcánica, Instituto Costarricense de Electricidad (ICE), Apdo. 10032-1000, Costa Rica.*

[4]*Terra Cognita Consultores S.A., Apdo 360-2350, Costa Rica*

*Corresponding autor, e-mail: mauricio.mora@ucr.ac.cr

## ABSTRACT

Arenal volcano is a small (~1750 m a.s.l., ~10 $km^3$) stratovolcano that continuously erupted between July 1968 and October 2010. During this long-lasting eruption (over 42 years), a large volume of material – about 5.6 x $10^8$ $m^3$ of dense rock equivalent – has been extruded and has produced a thick and extended lava field, mainly on the western flank of the edifice. Measurements of ground deformation obtained using a network of dry-tilt stations are presented for the period 1986-2000. They show a continuous subsidence of the volcano with maximal amplitude on the western side. The load effect of the lava field is calculated and explains the largest part of the observed tilts. Once the data are corrected by this load effect, pressure source models are not supported by the observations and by quality criteria on the models. Although the dry tilt data from Arenal volcano give limited constraint on the deformation models, they are representative of a long period of activity that cannot be recovered by other means. Moreover, the corresponding interpretative model is consistent with results obtained by geotechnical studies and modern ground deformation methods like InSAR.

## INTRODUCTION

Ground deformation study is, along with seismology and remote sensing of volcanic gases, one of the most common and widely used disciplines applied to research and monitoring of volcanoes. It can give important constrains on many volcanological problems such as magma storage and transport to the surface and instability of the volcano flanks. Geodetic techniques used on volcanoes have greatly evolved from man dependent methods (levelling, electronic distance measurement, dry tilt) to automatic ones (GPS, electronic tiltmeters), offering possible real-time measurements, and to satellite remote sensing techniques, like Synthetic Aperture Radar interferometry (InSAR), that allow measurement of the overall deformation field. Application of these techniques depends, of course, on economic and logistical constraints. For example, many active volcanoes are located in tropical environments which

pose many difficulties to geodetic techniques, either on land or from space, because of the weather conditions (i.e. frequent cloud cover), vegetation and high erosion rates.

One of the first ground deformation studies applied to active volcanoes in Costa Rica, is linked to the onset of Arenal eruption in July 29$^{th}$ 1968 and the interest of Costa Rican Institute of Electricity (ICE) to monitor the volcano due to its proximity to a hydroelectrical power plant site. Arenal is a small (~1750 m a.s.l., ~10 km$^3$) and young (~7000 years old) stratovolcano that has been continuously erupting since the series of explosions, beginning on July 29$^{th}$ 1968, that formed 3 new craters (A, B and C, from lower to upper). Those craters together with the former crater D, lie on an E-W fissure system (Fig. 1). From September 1968 to 1974, effusive activity from crater A produced a basaltic-andesitic lava field on the western flank. In 1974, the activity migrated to crater C, forming a new cone on the western flank of the edifice. Since then, there was a lava pool at crater C (Alvarado and Soto, 2002), where rare and transient lava domes and hornitos (or a combination of both) were formed. Aa lava flows have also been erupted almost continuously from the lava pool, changing to blocky lava flows downslope (Borgia and Linneman, 1980; Wadge, 1983). The lava field extruded since 1974 from crater C has partly overlapped the previous lava field produced by crater A. Up to now, Arenal has erupted for over 42 years, totaling ~0.70 km$^3$ of lava and tephra (~0.56 km$^3$ Dense Rock Equivalent - DRE), weighing ~1.4 x 10$^{12}$ kg, over a surface of about 7.5 km$^2$ with a maximum thickness of ~150-200 m. Up to the year 2000 (the end of our period of analysis), the volume and weight were about 0.54 km$^3$ DRE and 1.35 x 10$^{12}$ kg, respectively (Wadge et al., 2006).

Strombolian activity began in 1984 (Borgia et al., 1988; Barquero et al., 1992). However, since 1987 it changed to Vulcanian eruptions with infrequent pyroclastic flows originating from column collapse, lava front collapse and lava pool collapse. The major pyroclastic flow events occurred in June 1975, August 1993, May 1998, August 2000, and March 2001 (Alvarado and Soto, 2002) and smaller ones in September 2003, September 2007, June 2008, June-July 2009 and March 2010. Since 1998, the activity at crater C changed from very explosive to more effusive. Consequently, this crater grew several tens of meters and the lava pool was replaced by a viscous lava crust with dome-like structures leading to lava flows, up to October 2010. Since then, volcanic activity decreased substantially with practically no explosive events and minimal seismic activity.

The first measurements carried out to detect and observe volcanic deformation at Arenal were performed in 1969 (from September 11$^{th}$ to December 14$^{th}$) using a diamagnetic tiltmeter that was located 3.5 km NNW of the active crater A (Sawdo and Simon, 1969; Simon et al., 1970). Tiltgrams showed deflation and inflation on the order of 10 μrad. After that, ICE built four optical leveling (dry tilt) stations along a radial line on the west flank of Arenal. The data obtained from those dry tilt stations for the period 1976 to 1978, were analyzed by Melson et al. (1979). This dry tilt network was extended in 1985 by six additional stations installed on the northern and eastern flanks. Although some stations have been destroyed by lava flows, pyroclastic flows or erosion, very long-duration data series have been obtained. The long-term deformation revealed by this network correspond to a deflation of the volcano. This trend has been confirmed by other geodetic studies, such as that of Van der Laat (1988) from July 1982 to 1988. Later, Hagerty et al. (1997) carried out the first continuous GPS measurements at Arenal, observing a shortening of 7.5 ± 0.4 mm/yr (mm yr$^{-1}$) from May 1995 to March 1997 along a N-S baseline.

Two main hypotheses have been proposed to explain the long term subsidence of Arenal. First, following the most common model to explain deflation on volcanoes, Simon et al. (1970), Melson et al. (1979), Van der Laat (1988) and Hagerty et al. (1997) interpreted the deformation as the result of the depressurization of a very shallow magma chamber about 1 km in diameter, with depths between 0.8-1.5 and 4 km. Second, Wadge (1983), Alvarado et al. (1988), Soto (1991), Mora (2003), and Alvarado et al. (2003) proposed as an alternate explanation, the response to the load produced by the lavas emplaced since 1968. Indeed, post-eruptive deformation related to emplacement of lava fields have been detected by geodetic and remote sensing measurements at Sakurajima volcano (Ishihara et al., 1981), Piton de la Fournaise (Delorme, 1994), and Etna (Murray, 1988; Briole et al., 1997). Moreover, Grapenthin et al. (2010) demonstrated that it is important to correct the observed deformation from the load effect prior to any estimation of pressure source parameters. Recently, two studies brought new insights on Arenal deformation. Alvarado et al. (2010) speculated on an incipient deformation stage generated by spreading of the basement composed of weathered volcanic (mostly epiclastics) rocks strongly lateritized. Ebmeier et al. (2010) interpreted InSAR measurements as a steady downslope movement on the western flank.

In this paper, we present the dry tilt network and the observations obtained from 1986 to 2000. Following the approach of Grapenthin et al. (2010), we estimate the deformation produced by the load of lava emplaced from 1988 to 2000 and compare them to the tilt measured in the same interval. Then, by using numerical methods, we investigate the ability of the pressure source model to explain the observed deformations corrected by the load effect. Finally, we open a discussion on the possible origins of the long-term subsidence at Arenal volcano.

## DESCRIPTION OF THE TILT STATIONS AND OBSERVATIONS

### The dry tilt network

ICE adopted the dry tilt technique developed at the Hawaiian Volcano Observatory in the late 1960s (Kinoshita et al., 1974) and following studies (Sylvester, 1978; Yamashita 1981). The first 4 dry-tilt stations (A, B, C and D) were set up on the western flank of Arenal in October 1974 (Fig. 1). Station A was covered by a lava flow on January 29th 1977, then in 1985, a year after the beginning of the explosive phase, six other stations (E, F, G, I, J and K) were installed on the eastern and northern flanks of the volcano, completing a network of 9 dry-tilt stations.

The stations are composed of benchmarks forming 40-m-side triangles (stations E, F, G, I, J and K) and squares (stations C and D) with a reference point at the center. These last stations consist of two triangular sub-arrays called C1 and C2, and D1 and D2 (see Table 1). The benchmarks are stainless steel rods (2.5 cm in diameter and 3-6 m long) placed in holes cemented with concrete, leaving only 5 cm of the rod above the surface. The top of each rod is rounded and protected to prevent corrosion.

On each flank, the different sets of stations were built following radial lines from the active crater. Volcanic and human activity, though, destroyed part of the network. Station B collapsed by erosion along a contiguous gully in 1991, but serious damage was already visible by late 1990. Station C was damaged by the August 28$^{th}$ 1993 pyroclastic flow and was repaired some months later. However, one of the benchmarks was eroded and measurements

at sub-array C2 stopped in 1995. Station G was unintentionally destroyed by local people in 1999 and station E was covered by the August 23rd 2000 pyroclastic flow.

**Dry tilt data set**

Measurements were usually carried out every three to four months using an optical level and a 3 m long Kern invar rod. However, logistical and economic problems sometimes increased this measurement interval and, for some years, only two or one measurement is available. The local tilt is calculated following the method proposed by Yamashita (1981). The standard error of the tilt is about 2 μrad, but frequently 3-5 μrad according to experience in Iceland although larger errors ocurr if the rods are not well coupled to the surrounding rock or soil (Tryggvason et al., 1994). At Arenal, all the stations are constructed on tephra and epiclastic deposits because of the absence of solid rock, which may induce local instabilities.

The total accumulated tilt vectors obtained from the ICE's dry tilt data set from 1988 to 2000, show an overall pattern of tilt down towards the west flank of Arenal volcano, except for station E, which is anomalous in direction and magnitude (Fig. 1). The amplitude of the down-tilt observed is larger at stations close to the summit and those at western flank (Fig 1, Table 1). In fact, the tilt vectors at stations J, G, F, B and D are mainly directed to the NW flank of the volcano. Figures 2 and 3 display the temporal variations of the tilt vectors and amplitudes, respectively. It can be observed that the direction of the vectors at stations E and F are quite constant. For stations G, I, J, and K, the tilt directions are also relatively constant, although the signal to noise ratios are much lower. At station C, the directions obtained for the two sub-arrays are similar and constant until 1997. After that, the direction of the vector at C1 is strongly modified. Sub-array D2 also appears to be perturbed, while D1 is stable with a constant tilt direction. At almost all the stations, the tilt amplitude varies approximately linearly with the cumulate volume of magma emitted (Fig. 3) indicating a progressive source process. Hence, the tilt rates tend to progressively decrease together with the extrusion rate. The highest tilt rate is observed at station B until it was damaged in 1990.

Superposed on the long-term down-tilt, there are short-term variations that are not coherent among the stations. Those variations can result from perturbations produced by non-volcanic processes (i.e., charge and discharge of water, temperature changes). However, the lack of complementary continuous deformation and meteorological data as well as detailed knowledge of the response of each station site makes it difficult to discriminate external effects from the volcanic signals. Hence those variations are not considered in this work.

**DEFORMATION MODELLING**

**Quality criteria of models**

To evaluate the goodness of models, several complementary criteria are used. The first one is the significance of the models from a physical and volcanological point of view. Unrealistic models must be discarded even if they explain well the data. The second criterion is a misfit function between the observed and calculated tilts. Here we use the error function defined as:

$$\chi^2 = \sum_{i=1}^{N} \left( \frac{t_c^i - t_o^i}{\sigma^i} \right)^2 \quad (1)$$

where $N$ is the number of data (twice the number of dry tilt stations as tilts are two-components vectors), $t_o^i$ and $t_c^i$ are the observed and calculated tilts, and $\sigma^i$ is the standard error assigned to the datum. This error includes measurement uncertainties, different kinds of perturbation such as monument instabilities, and modelling error due for example to over-simplification of the models. Here we take $\sigma^i = \sigma_0 = 20\,\mu rad$ for all stations and components. In order to compare models that have different numbers of parameters, we use also the Akaike Information Criteria (AIC – Akaike, 1974) to test their statistical significance and measure the improvement when more parameters are added. The AIC is defined as $AIC = 2p - 2\ln L$, where $p$ is the number of parameters and $L$ is the likelihood of the model:

$$L = \left(2\pi\sigma_0^2\right)^{-N/2} \cdot \exp\left(-\frac{\chi^2}{2}\right) \quad (2).$$

The AIC can be rewritten as:

$$AIC = 2p + N\ln\left(2\pi\sigma_0^2\right) + \chi^2 \quad (3).$$

In our case, where the number of data, N, is small, it is convenient to use a corrected Akaike Information Criteria (Burnham and Anderson, 2002):

$$AICc = AIC + \frac{2p(p+1)}{N-p-1} \quad (4).$$

**Mechanical parameters**

The numerical models used below require as inputs several mechanical characteristics of the medium such as density $\rho$, Poisson ratio $\nu$, and Young's modulus $E$. On the basis of field observations and measurements on samples, the global porosity of the lava field material was estimated in the range 30 to 35%. Thus, taking a density of 2500 kg $m^{-3}$ for an andesitic dense rock, an average density of 1700 kg $m^{-3}$ was obtained for the lava field (Alvarado et al., 2006). The real medium is a heterogeneous stratified structure. Its elastic coefficients and seismic velocities strongly vary with depth. Mora et al. (2006) obtained velocity models at Arenal by using the SPAC method (Aki, 1957). The estimated S-wave velocities vary from about 300 $m^1\,s^{-1}$, in the first 10 meters of the structure, to ~1500 $m^1\,s^{-1}$ for depth greater than 300 m. The Young's modulus can be estimated from $Vs$ with the relation $E = 2\rho V_S^2(1+\nu)$. Taking $\nu = 0.25$, this yields a range of values for $E$ from 1 to 14 GPa. Since this parameter is poorly known, we will explore the model space using 4 values of $E$ (1.2, 4, 9, and 14 GPa) in the models. These values are consistent with the estimations of $E$ for pyroclastic rocks of Arenal (Alvarado et al., 2010).

**Effect of lava load**

As noted above, Arenal has produced large quantities of pyroclastic material and lava that lie on the flanks. Wadge et al. (2006) obtained relatively precise isopach maps for several periods since 1968. The period from 1988 to 2000 was taken for this work because the best data set is complete for this period, both from lava production (Table 2) and deformation.

From 1968 to 1988, 42.6 x $10^7$ $m^3$ DRE were extruded, while 11.4 x $10^7$ $m^3$ DRE were emitted in 1988-2000 (Table 2; Wadge et al., 2006, Hofton et al., 2006). Following the procedure of Grapenthin et al. (2010), it is thus possible to estimate and take into account the ground deformations produced by the surface load of lava. We adopted the approach presented by Pinel et al. (2007) to study surface displacements generated by ice load variations at Katla volcano, Iceland. The vertical and horizontal radial displacements of the surface, induced by a unit point mass applied on an elastic half-space are given by:

$$\begin{aligned} U_z(r) &= \frac{g}{\pi}\frac{1-\nu^2}{E}\frac{1}{r} \\ U_r(r) &= -\frac{g}{2\pi}\frac{(1+\nu)(1-2\nu)}{E}\frac{1}{r} \end{aligned} \quad (5)$$

where $g$ is gravity and $r$ is the distance to the source (Sneddon, 1951). The components of the corresponding tilt vector in Cartesian coordinates are:

$$\begin{cases} \dfrac{\partial U_z}{\partial x} = -\dfrac{g}{\pi}\dfrac{1-\nu^2}{E}\dfrac{x}{r^3} \\ \dfrac{\partial U_z}{\partial y} = -\dfrac{g}{\pi}\dfrac{1-\nu^2}{E}\dfrac{y}{r^3} \end{cases} \quad (6)$$

with $r = \sqrt{x^2 + y^2}$ . These derivatives can be considered as Green functions. In order to obtain the tilt produced by a lava flow load, the Green functions are convolved by the mass distribution:

$$\begin{cases} t_x(\vec{r}) = \displaystyle\int_S \frac{\partial U_z}{\partial x}(\vec{r}-\vec{r}\,') \cdot \rho(\vec{r}\,') \cdot h(\vec{r}\,') \cdot d\vec{r}\,' \\ t_y(\vec{r}) = \displaystyle\int_S \frac{\partial U_z}{\partial y}(\vec{r}-\vec{r}\,') \cdot \rho(\vec{r}\,') \cdot h(\vec{r}\,') \cdot d\vec{r}\,' \end{cases} \quad (7)$$

where $\rho$ and $h$ are the density and thickness of the lava deposit, respectively, and the integration is carried out over the whole area $S$ of the lava field.

Table 3 shows the misfit $\chi^2$ and AICc obtained for the tilts associated to surface load. The best fit is obtained for $E$ = 1.2 GPa. For higher values of $E$, the load effect decreases and does not account for the observations. We verified also that lower values of $E$ yield worse fitting. Figure 4 displays the observed tilts vectors and those calculated with $E$ = 1.2 GPa.

**Pressure source model**

The deformation produced by pressure variations in a spherical source embedded in an elastic half-space can be calculated analytically (Mogi, 1958). However, caution has to be taken in presence of topography which may have a strong influence on tilt when the flanks of the volcano are steep. Cayol and Cornet (1998) showed that, for slopes greater than 20°, the direction of the tilt can even be reversed and hence, it is important to take topography into account when modeling the deformations. At Arenal, only tiltmeters D, G and K, are located at sites with slope less than 20°.

We calculated the strain and stress perturbations by using the Finite Element Method. An axi-symetrical geometry includes an azimuthally average topography of Arenal. In order to avoid border effects, the computing domain is much larger than the volcano. It is a cylinder with radius of 100 km and depth of 100 km including about $10^4$ triangular elements. The source is a cavity at depth in which a pressure variation is applied. It is spherical or ellipsoidal. Figure 5 presents the geometry of the model. We compared the results of the FEM calculations with the analytical solution of Mogi (1958) model for plane topography. For distances larger than 2000 m, the two models give similar tilts, while they significantly differ at shorter distance from the crater.

In the case of a spherical cavity, the pressure source model is characterized by 2 parameters, its depth $H_c$ and radius $R_c$. The parameter space is explored in the ranges 0 to 5000 m for $H_c$ and 100 to 600 m for $R_c$. For each value of the point ($H_c$, $R_c$), the pressure variation that produces the best fit between the observations and the sum of the tilts associated to the surface load and to the chamber model is estimated. Figure 6 and Table 3 shows the results obtained for the 4 values of $E$. It can be observed that the misfit does not depend on the radius and only varies slightly with depth. Although minimum misfits are obtained at depths of 500 m below sea level (i.e., 2000 m below the crater) for $E \geq 4$ GPa, this parameter is poorly constrained. For $E$ = 1.2 GPa, the depth of the cavity is greater than 3000 m. The optimal pressure variation $\Delta P$ is always negative (depressurization) and strongly depends on the radius. This is similar to the Mogi (1958) model in which ground deformations are proportional to $R_c^3 \Delta P$. In the case $E$ = 1.2 GPa, very low pressure variations are obtained which corresponds to very small surface deformations. Thus, the pressure source barely improves the fit. When $E$ increases, the medium is more and more rigid, the load effect alone no longer account for the observed tilts and a chamber with larger and larger pressure variations must be added to fit the data. The best fitting ($\chi^2$= 37, Table 3) is obtained for $E$ = 1.2 GPa. The misfit $\chi^2$ increases when $E$ becomes larger. For high Young's modulus, the superposition of the lava load and pressure source models yields better fits than the load effect alone. However, for $E$ = 1.2 GPa, although $\chi^2$ is slightly better, the AICc increases from 122 to 126 due to higher number of parameters. Furthermore, the pressure decrease cannot exceed the lithostatic pressure at the level of the magma chamber. This rough constraint imposes a lower limit on the source radius (Fig. 6). For example, for E = 9 GPa, the radius must be greater than 500 m for an optimal depth of 2000 m below the crater. Thus, from the physical and volcanological points of view, the pressure source model appears to be unrealistic. Some calculations with an ellipsoidal chamber have also been carried out. For an oblate cavity, for example, with horizontal axis larger than the vertical axis, the pressure variation is slightly reduced, allowing a smaller radius, and the data fitting is somewhat improved. However the corresponding AICc is higher due to the increasing number of parameters of the model. Thus, in any of the cases, following most of the defined criteria, a pressure source is not required by the data. In summary, once the surface lava load is taken into account, the existence and effects of a shallow magma reservoir are really not supported by the observed tilts.

## DISCUSSION

Our results, based on 12 years of dry tilt measurements, demonstrate that the long lasting eruption of Arenal volcano is associated with a continuous subsidence with larger amplitude on the western flank. This general trend is also confirmed by recent GPS (del Potro and Muller, 2009) and InSAR (Ebmeier et al., 2010) measurements carried out on shorter time

scales. In order to understand the long term evolution of the ongoing eruption, it is thus important to identify the physical processes that can be related to the subsidence.

Considering the large volume and weight of material erupted over 42 years, we first analyze the effect of the surface load of those deposits. Using the precise isopach maps obtained for the period 1988-2000 by Wadge et al. (2006), a density $\rho$ = 1700 kg $m^{-3}$ and small Young modulus $E$ = 1.2 GPa, we obtain a relatively good fit between the calculated and observed tilts.

The other common source of deformation on volcanoes is the pressure variation in the magma chamber (e.g., Rymer and Williams-Jones, 2000; Lisowski, 2007; Kohno et al., 2008). Therefore, we also modelled a pressure source embedded in the structure, taking topography into account. We see that for low values of Young's modulus ($E$ = 1.2 GPa), the pressure source does not improve the fit already obtained by the load effect and is discarded by using the Akaike Information Criteria. For higher values of $E$, data fit is improved by considering the depressurization of a shallow reservoir (2000 m below the crater) with a radius larger than 350 to 550 m. Furthermore, this model requires a large pressure decrease, compared with the lithostatic pressure, which would have induced a strong reduction of the extrusion rate, in contradiction with observations. Consequently, our analysis demonstrates that a deflation of a shallow magma chamber is not the origin of the measured tilts. This result is consistent with geological (Wadge, 1983; Alvarado et al., 1988; Soto, 1991), petrological and geochemical considerations on a relatively deep chamber (Reagan et al., 1987; Sachs and Alvarado, 1996; Streck et al., 2005; Williams-Jones et al., 2001).

Using equation 5 and the lava thickness for the period 1988-2000, we also calculated the displacement resulting from the surface load. At about 1800 m west of the crater, close to dry tilt station C, the vertical displacement ranges from 8 cm (using $E$ = 4 GPa) to 26 cm ($E$ = 1.2 GPa). This corresponds to an average subsidence rate of 0.65 to 2.2 cm $yr^{-1}$ for this period. This rate can be compared to the downward displacement of about 2 cm $yr^{-1}$ estimated by InSAR data for the period from September 2007 to January 2008 at approximately the same area by Ebmeier et al. (2010). As the extrusion rate was much higher in 1988-2000 than during the later period, the real subsidence rate was probably larger than that calculated with the surface load. This rough comparison suggests that the load effect alone does not account completely for the observed subsidence. Non-elastic delayed deformation processes can also contribute to it.

For example, a geological and geotechnical study carried out by Alvarado et al. (2003, 2010) to characterize and understand the deformation processes of the basement and slopes of Arenal edifice showed that, at the sites of maximum lava thickness, the rate of subsidence would be 60 mm $yr^{-1}$, for a cumulated subsidence of ~2 m that represents only 18% of consolidation of the underlying units. They also suggested, according to their calculations, that the total subsidence will be about 19 m once the loading effect ceases (this may happen in one to several centuries according to the consolidation coefficient). At a larger scale, Alvarado et al. (2003, 2010) estimated that the Arenal edifice (1.1 km high, 10 $km^3$ of volume, ~20 x $10^3$ kPa) has produced a total subsidence of its basement up to 45 m for the last 7000 years. The large amplitude and long duration of the subsidence associated to the consolidation process suggests that this phenomenon could explain part of the present observations. In particular, the discrepancy between observed and calculated tilt vectors could be due to the consolidation of heterogeneous underlying layers at some stations, located at different active tectonic blocks.

Ebmeier et al. (2010) detected a downslope movement of the upper western flank of the volcano, with large horizontal components at the highest parts of the studied zone. They interpreted these deformations as creep along a shallow sliding plane. Along an E-W profile, their interferograms extend from about 800 m to 1900 m west from the crater, including the site of dry tilt station C. At this location, the displacements estimated by InSAR are almost vertical and downward, in agreement with our observations and models. This is also consistent with the studies of Alvarado et al. (2003, 2010) who concluded that spreading processes due to dispersion can affect Arenal volcano. It is thus probable that most of the vertical displacements detected by InSAR results from loading effects.

Finally, some discrepancies between the tilt vector calculated with the surface load model and the observed one, especially in their directions (Fig. 4), could result from local perturbations due to: monument instabilities, heterogeneities of the geological structure, proximity of a fault or proximity to a lava flow. Station E, for example, was very close to the N-S fault crossing the edifice (Fig. 1). As the corresponding tilt direction is constant and the amplitude is approximately proportional to the emitted volume, the observed deformation at station E can be interpreted as the result of a perturbation of the general tilt field by the fault. At some stations, nearby lava flows could also produce large misfit if its thickness and geometry are not precisely known.

## CONCLUSIONS

The long time series of dry-tilt data presented in this study clearly demonstrate a progressive subsidence of Arenal volcano with maximal amplitude on the western flank. We conclude it is related to the long-lasting eruption, that has produced about 5.6 x $10^8$ $m^3$ of lava and tephra, from which about 1.1 x $10^8$ $m^3$ DRE of material were produced between 1988 and 2000, with a total weight of 0.26 x $10^{12}$ kg. Thanks to the good knowledge of the distribution of this material, the effect of its load could be calculated by using an elastic structure. It appears to be predominant in the observed tilts. Models of pressure source have been superimposed on the load model; however they not improve significantly the fit between observed and calculated tilts and are not supported by the Akaike Information Criteria. Furthermore, although poorly constrained by the data, the corresponding features of a magma chamber – depth, radius, pressure variation – are not consistent with many volcanological data. Other phenomena, such as large-scale sliding, visco-elastic response to loading of the structure and basement of the volcano, settlement of material and local perturbations by structural heterogeneities and faults,

have probably some influence on the deformations. Long term deformation measurements after the end of the extrusion would be useful to follow the evolution of subsidence and to confirm, or not, our results and interpretation. Although the dry tilt data from Arenal volcano are of moderate quality and give limited constraint on the deformation models, they are representative of a long period of activity that cannot be recovered by other means. Moreover, the corresponding interpretative model is consistent with results obtained by geotechnical studies and modern ground deformation methods like InSAR. The use of other monitoring technologies, such as GPS, would help identifying the different sources of deformation at Arenal and give a new and wider insight on volcanic processes and hazards.

## ACKNOWLEDGMENTS

We are grateful to ICE for supporting the logistical work and the data acquisition. The financial support at different stages of the study was obtained from projects: 113-A4-501, 113-A6-503, 830-A7-511 and 113-B1-230 from University of Costa Rica. Support was also obtained by the European Commission 6th Framework Project VOLUME (Contract N° 018471). We thank Delioma Oramas Dorta for providing the isopach data of Arenal volcano lavafield. We thank Virginie Pinel for useful discussions and for providing some computer programs. We thank the contributions and guidance of Tim Dixon, Geoff Wadge, Rodrigo del Potro and Maurizio Battaglia during earlier stages of the manuscript. Comments and contributions from Glyn Williams-Jones and Hugo Delgado Granados greatly improve the present manuscript. We are also grateful to the Arenal Conservation Area staff for the facilities provided during the field work.

## REFERENCES CITED

Alvarado, G.E., Argueta, S., and Cordero, C., 1988, Interpretación preliminar de las deformaciones asociadas al Volcán Arenal (Costa Rica): Boletín del Observatorio Vulcanológico del Arenal, no. 2, p. 26-43.

Alvarado, G.E., 2000, Los volcanes de Costa Rica: geología, historia y riqueza natural: San José, Costa Rica, EUNED, 284 p.

Alvarado, G.E., and Soto, G.J., 2002, Pyroclastic flow generated by crater-wall collapse and outpouring of the lava pool of Arenal Volcano, Costa Rica: Bulletin of Volcanology, v. 63, no. 8, p. 557-568.

Alvarado, G.E., Carboni, S., Cordero, M., Avilés, E., Valverde, M., and Leandro, C., 2003, Estabilidad del cono y comportamiento de la fundación del edificio volcánico del Arenal (Costa Rica): Boletín del Observatorio Sismológico y Vulcanológico de Arenal y Miravalles, no. 26, p. 21-73.

Alvarado, G.E., Carboni, S., Cordero, M., Avilés, E., and Valverde, M., 2010, Stability of the cone and foundation of Arenal volcano, Costa Rica, *in* Olalla, C., Hernández, L.E., Rodríguez-Losada, J.A., Perucho, A. and González-Gallego, J., eds., Volcanic Rock Mechanics: Rock Mechanics and Geo-engineering in Volcanic Environments: London, Taylor and Francis Group, p. 135 – 150.

Akaike, H., 1974, A new look at the statistical model identification: IEEE Transactions on Automatic Control, v. 19, no. 6, p. 716–723.

Aki, K., 1957, Space and time spectra of stationary stochastic waves, with special reference to microtremors: Bulletin of the Earthquake Research Institute, v. 35, p. 415–456.

Barquero, R., Alvarado, G.E., and, Matumoto, T., 1992, Arenal Volcano (Costa Rica) Premonitory Seismicity, *in* Gasparini, P., Scarpa, R., and Aki, K., eds., Volcanic Seismology. IAVCEI Proceedings in Volcanology Series, v. 3, Berlin, Springer-Verlag, 572 p.

Borgia, A., and Linneman, S.R., 1980, On the Mechanisms of Lava Flow Emplacement and volcano Growth: Arenal, Costa Rica, *in* Fink, J.H., ed., Lava Flows and Domes Emplacement Mechanisms and Hazard Implications. IAVCEI Proceedings in Volcanology, v. 2, Berlin, Springer-Verlag, p. 208-243.

Borgia, A., Poore, C., Carr, M.J., Melson, W.G., and Alvarado, G.E., 1988, Structural, stratigraphic and petrologic aspects of the Arenal-Chato volcanic system, Costa Rica: Evolution of a young stratovolcanic complex: Bulletin of Volcanology, v. 50, no. 2, p. 86-105.

Burnham, K. P., and Anderson, D.R., 2002, Model Selection and Multimodel Inference: A Practical Information-Theoretic Approach: New York, USA, Springer-Verlag, 488 p.

Briole, P., Massonnet, D., and Delacourt, C., 1997, Post-eruptive deformation associated with the 1986-87 and 1989 lava flows of Etna detected by radar interferometry: Geophysical Research Letters, v. 24, no. 1, p. 37-40.

Cayol, V., and Cornet, F.H., 1998, Effects of topography on the interpretation of the deformation field of prominent volcanoes - Application to Etna: Geophysical Research Letters v. 25, p. 1979-1982.

Delorme, H., 1994, Apport des déformations à la compréhension des mécanismes éruptifs: le Piton de la Fournaise [Thèse d'Etat]: Paris, Université Paris VII, p. 449-467.

Del Potro, R., and Muller, C., 2009, Enhanced three-dimensional stochastic adjustment form combined volcano geodetic networks [abs.]: American Geophysical Union, Fall Meeting 2009, AGUFM.G41A0699D.

Ebmeier, S.K., Biggs, J., Mather, T.A., Wadge, G., and Amelung, F., 2010, Steady downslope movement on the western flank of Arenal volcano, Costa Rica: Geochemmistry Geophysics Geosystems, v. 11, no 12, Q12004, doi:10.1029/2010GC003263.

Grapenthin, R., Benedikt, G.O., Sigmundsson, F., Sturkell, E., and Hooper, A., 2010, Pressure sources versus surface loads: Analyzing volcano deformation signal composition with an application to Hekla volcano, Iceland: Geophysical Research Letters, v. 37, L20310, doi:10.1029/2010GL044590.

Hagerty, M.T., Schwartz, S.Y., Protti, M., Garcés, M., and Dixon, T., 1997, Observations at Costa Rican volcano offer clues to causes of eruptions: Eos (Transactions, American Geophysical Union), v. 78, no. 49, p. 570-571.

Hofton, M. A., Malavassi, E., and Blair, J. B., 2006, Quantifying recent pyroclastic and lava flows at Arenal Volcano, Costa Rica, using medium-footprint lidar: Geophysical Research Letters, 33, L21306, doi:10.1029/2006GL027822.

Ishihara, K., Takayama, T., Tanaka, Y., and Hirabayashi, J., 1981, Lava flows at Sakurajima Volcano (I) -volume of the historical lava flows: Annals of Disaster Prevention Research Institute, Kyoto University, 24-B-1, p. 1-10. (In Japanese).

Kinoshita, W.T., Swanson, D.A., and Jackson, D.B., 1974, The measurement of crustal deformation related to volcanic activity at Kilauea Volcano, Hawaii, *in* Civetta, L., Gasparini, P., Luongo, G., and Rapolla, A., eds., Physical Volcanology: Amsterdam, Elsevier, p. 87-115.

Kohno, Y., Matsushima, T., and Shimizu, H., 2008, Pressure sources beneath Unzen Volcano inferred from leveling and GPS data: Journal of Volcanology and Geothermal Research, v. 175, p. 100–109, doi:10.1016/j.jvolgeores.2008.03.022.

Lisowski, M., 2007, Analytical volcano deformation source models, *in* Dzurisin, D., 2007, Volcano deformation – geodetic monitoring techniques, Chichester, UK, Springer-Praxis Publishing Ltd., p. 279-304.

Melson, W.G., Umaña, J., and Evans, E., 1979, Arenal volcano: Results of dry tilt measurements: SEAN Bulletin, v. 4, no. 2, p. 13-16.

Mogi, K., 1958, Relations between the eruptions of various volcanoes and the deformation of the ground surfaces around them: Bulletin of the Earthquake Research Institute, v. 36, p. 99-134.

Mora, M., 2003, Étude de la structure superficielle et de l'activité sismique du volcan Arenal, Costa Rica [Ph.D. thesis]: Chambéry, Universite de Savoie, 155 p.

Mora, M. M., Lesage, P., Valette, B., Alvarado, G. E., Leandro, C., Métaxian, J.-P., and Dorel, J., 2006, Shallow velocity structure and seismic site effects at Arenal volcano, Costa Rica: Journal of Volcanology and Geothermal Research, v. 152, p. 121–139, doi: 10.1016/j.jvolgeores.2005.09.013.

Murray, J.B., 1988, The influence of loading by lavas on the siting of volcanic eruption vents on Mt Etna: Journal of Volcanology and Geothermal Research, v. 35, p. 121-139, doi:10.1016/0377-0273(88)90010-8.

Pinel, V., Sigmundsson, F., Sturkell, E., Geirsson, H., Einarsson, P., Gudmundsson, M. T., and Högnadóttir, T., 2007, Discriminating volcano deformation due to magma movements and variable surface loads: application to Katla subglacial volcano, Iceland: Geophysical Journal International, v. 169, no. 1, p. 325-338, doi: 10.1111/j.1365-246X.2006.03267.x

Reagan, M.K., Gill, J.B., Malavassi, E., and García, M.O., 1987, Changes in magma composition at Arenal volcano, Costa Rica, 1968-1985: Real-time monitoring of open system differentiation: Bulletin of Volcanology, v. 49, no. 1, p. 415-434.

Rymer, H., and Williams-Jones, G., 2000, Volcanic eruption prediction: Magma chamber physics from gravity and deformation measurements: Geophysical Research Letters, v. 27, no. 16, p. 2389–2392.

Sachs., P.M. and Alvarado, G.E., 1996, Mafic metaigneuos lower crust beneath Arenal volcano (Costa Rica): evidence from xenoliths: Boletín del Observatorio Vulcanológico del Arenal, no. 11-12, p. 71-78.

Sawdo, R.M., and Simon, I., 1969, Tiltmeter installation at Arenal volcano in Costa Rica: Report Arthur D. Little Inc., Cambridge, U.S.A., 7 p.

Simon, I., Sawdo, R.M., Sáenz, R., and Melson, W.G., 1970, Preliminary results from tiltmeter recording at Arenal volcano, Costa Rica: Report Arthur D. Little Inc., Cambridge, U.S.A., 18 p.

Sneddon, I. N., 1951, Fourier transforms: New York, Mc Graw-Hill, 542p.

Soto, G.J., 1991, Análisis de la inclinometría seca en el volcán Arenal, 1988-90: Boletín del Observatorio Vulcanológico del Arenal, no. 9-10, p. 7-23.

Soto, G.J., and Arias, J.F., 1998, Síntesis de la actividad del volcán Arenal, año 1996: Boletín del Observatorio Vulcanológico del Arenal y Miravalles, no. 17-18, p. 11-18.

Streck, M. J., M. A. Dungan, F. Bussy, and E. Malavassi, 2005, Mineral inventory of continuously erupting basaltic andesites at Arenal volcano, Costa Rica: Implications for interpreting monotonous, crystal-rich, mafic arc stratigraphies: Journal of Volcanology and Geothermal Research, v. 140, p. 133–155, doi:10.1016/j.jvolgeores.2004.07.018.

Sylvester, A.G., 1978, The dry tilt method of measuring crustal tilt: U.S. Geological Survey Open-File Report 79-370.

Tryggvason, E., Alves, M.M., Alves, J.L., Nunes, J.C., and Ólafsson, H., 1994, Furnas volcano ground deformation measurements 1991-1993: Nordic Volcanological Institute Report 9401, University of Iceland, 19 p.

Van der Laat, R., 1988, Deformaciones asociadas al vulcanismo activo de Costa Rica entre 1981 y 1988: Costa Rican Volcanism Workshop, 13-18 November, Shenandoah National Park, 12 p.

Wadge, G., 1983, The magma budget of Volcán Arenal, Costa Rica, from 1968 to 1980: Journal of Volcanology and Geothermal Research, v. 19, p. 281-302, doi:10.1016/0377-0273(83)90115-4.

Wadge, G., Oramas Dorta, D., and Cole, P.D., 2006, The magma budget of Volcán Arenal, Costa Rica from 1980 to 2004: Journal of Volcanology and Geothermal Research, v. 157, p. 60-74, doi:10.1016/j.jvolgeores.2006.03.037

Williams-Jones, G., Stix, J., Heiligmann, M., Barquero, J., Fernandez, E., and Duarte Gonzalez, E. (2001) A model of degassing and seismicity at Arenal volcano, Costa Rica; Journal of Volcanology and Geothermal Research, v. 108, p. 121-141.

Yamashita, K.M., 1981, Dry tilt: a ground deformation monitor as applied to the active volcanoes of Hawaii: U.S. Geological Survey Open-File Report 81-523.

**Figure captions**

Figure 1: Arenal volcano in its tectonic framework (inset). Main faults labeled: ARF, Aguacaliente River Fault; DF, Danta Fault. Dotted lines: faults covered by the lava field. Craters, 1968-2009 lava field, location of the dry tilt meters and corresponding tilt vectors used in this work. Local coordinates Lambert Costa Rica North.

Figure 2. Path of tilt vectors for three consecutive periods. For C and D tiltmeters, black and gray traces correspond to measurements carried out at C1 and D1, and C2 and D2 subarrays, respectively.

Figure 3. Amplitude of cumulative tilt vectors. Bottom panels are: first, effusion rate based on data obtained from Soto and Arias (1998) and Wadge et al. (2006), second, cumulated volume (DRE) of magma calculated from effusion rate estimation.

Figure 4. Observed tilt vectors for period 1988-2000 (thin black arrows) and tilts calculated with: A) surface load model alone (thick black arrows), using E = 1.2 GPa, B) combining load and pressure source models (thick black arrows). Vectors obtained from both models are very close to each other due to great similarity of two sets of calculated tilts. Light gray contours: isopach map of the lava flow effused from 1988 to 2000 with contour levels every 20 m.

Figure 5: Sketch of pressure source model. Spherical cavity with radius $R_C$ embedded at elevation $H_C$ over sea level. Axi-symetrical representation of Arenal topography used in mechanical model.

Figure 6. Pressure source models for different values of Young's modulus. Pressure variation that produces best fitting is plotted as a function of elevation (a.s.l.) and radius of magma chamber. Gray color scale ~~is~~ logarithmic ~~and it is different for case E = 1.2 GPa.~~ Corresponding misfit values between observed tilts and tilts calculated with both load and pressure source models are displayed as black solid lines. Models with pressure variation higher than lithostatic pressure, indicated by ~~black~~ dotted lines, are unrealistic.

TABLE 1. CUMULATED TILTS FROM 1986 TO 2000.

| Station | Radial distance to active crater (km) | Down-tilt amplitude (μrad) | Azimuth | Duration of observation (months) |
|---|---|---|---|---|
| B | 1.5 | 235 | 52 | 45.4[a] |
| C1 | 1.9 | 253 | 113 | 178.2 |
| C2 | 1.9 | 196 | 81 | 106.2[b] |
| D1 | 3.1 | 49 | 73 | 178.2 |
| D2 | 3.1 | 103 | 61 | 178.2 |
| E | 2.0 | 390 | 286 | 170.6[c] |
| F | 2.7 | 129 | 220 | 178.2 |
| G | 3.3 | 79 | 237 | 158.0[d] |
| I | 2.3 | 97 | 308 | 178.2 |
| J | 2.8 | 49 | 245 | 178.2 |
| K | 3.5 | 58 | 326 | 178.2 |

*Notes:* a: B was destroyed in 1990. b: C2 data are not included after its reconstruction in 1994. c: E was destroyed in 2000. d: G was destroyed in 1999.

TABLE 2. VOLUME (DENSE ROCK EQUIVALENTS), WEIGHT AND PROPORTION OF LAVA EMITTED AT DIFFERENT PERIODS (DATA ADAPTED FROM WADGE ET AL., 2006).

| Period | Volume ($10^6$ $m^3$, DRE) | Weight ($10^{12}$ kg) | % |
|---|---|---|---|
| 1968 - 1988 | 426 | 1.07 | 76 |
| 1988 - 2000 | 114 | 0.29 | 21 |
| 2000 - 2009 | 20 | 0.05 | 3 |
| Total | 560 | 1.41 | 100 |

TABLE 3. MISFIT, $\chi^2$, AND CORRECTED AKAIKE INFORMATION CRITERIA, AICC, OBTAINED FOR 1) SURFACE LAVA LOAD AND 2) LAVA LOAD + PRESSURE SOURCE MODELS, USING DIFFERENT YOUNG´S MODULUS VALUES. OPTIMAL ELEVATION, $H_C$, AND MINIMAL RADIUS, $R_C$, OF MAGMA CHAMBER ARE ALSO GIVEN.

| Young's Modulus | Lava load | | Lava load + pressure source | | | |
|---|---|---|---|---|---|---|
| *E* (GPa) | $\chi^2$ | AICc | $\chi^2$ | AICc | $H_c$ (m) | $R_c$ min (m) |
| 1.2 | 42 | 122 | 37 | 126 | -3000 | 200 |
| 4 | 125 | 205 | 51 | 141 | -700 | 350 |
| 9 | 161 | 241 | 56 | 146 | -500 | 500 |
| 14 | 172 | 252 | 58 | 147 | -500 | 550 |

Mauricio M. Mora - Figure 1 - Figure 1.cdr

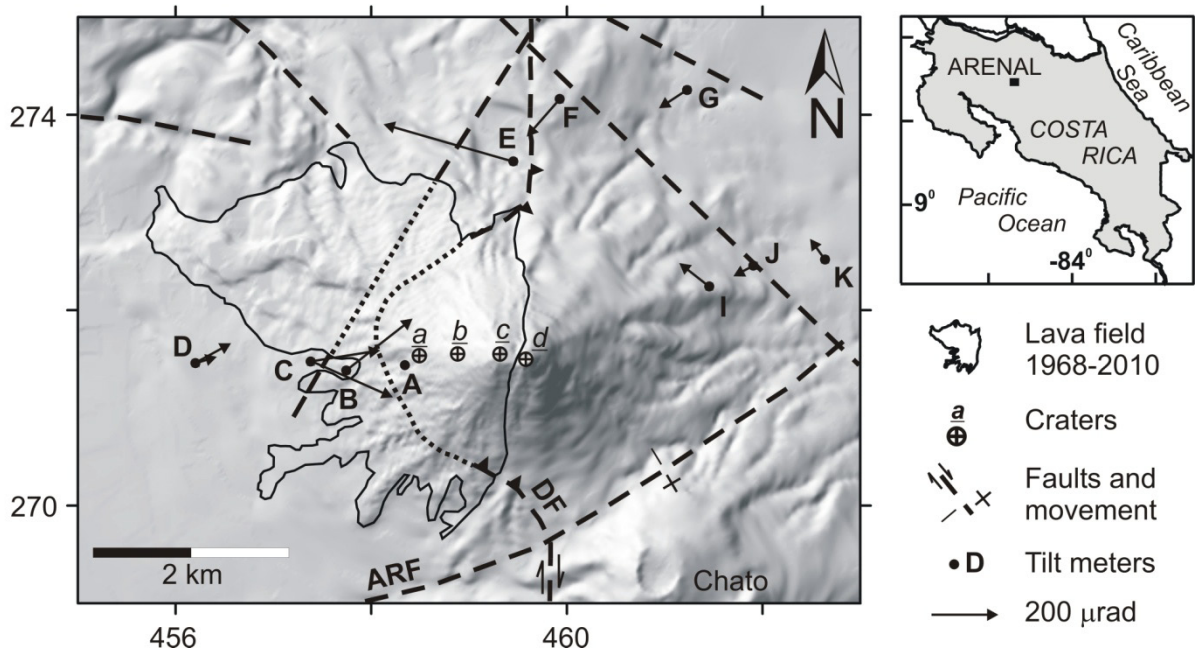

Mauricio M. Mora - Figure 2 - Figure 2.ai

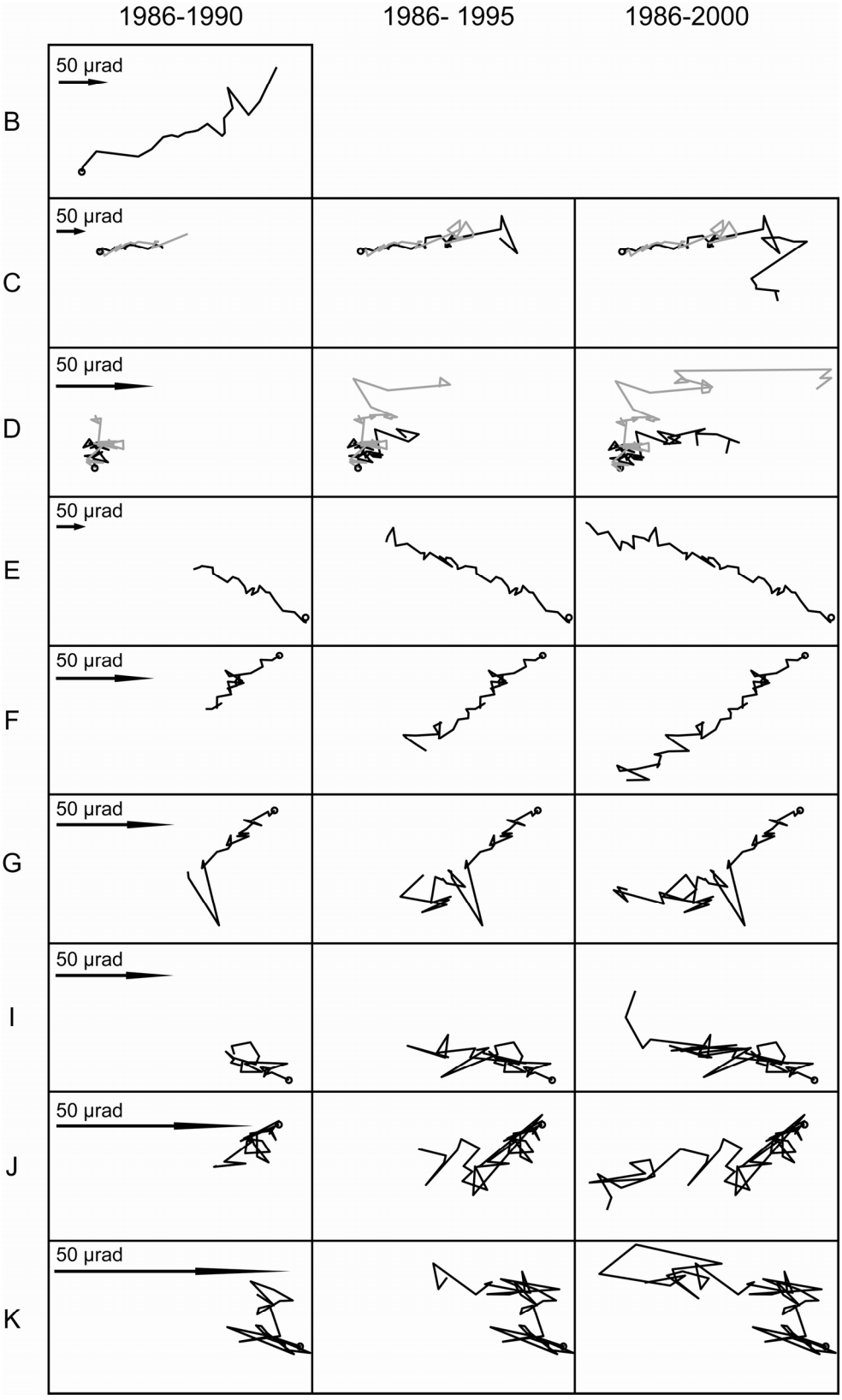

Mauricio M. Mora - Figure 3 - Figure 3.ai

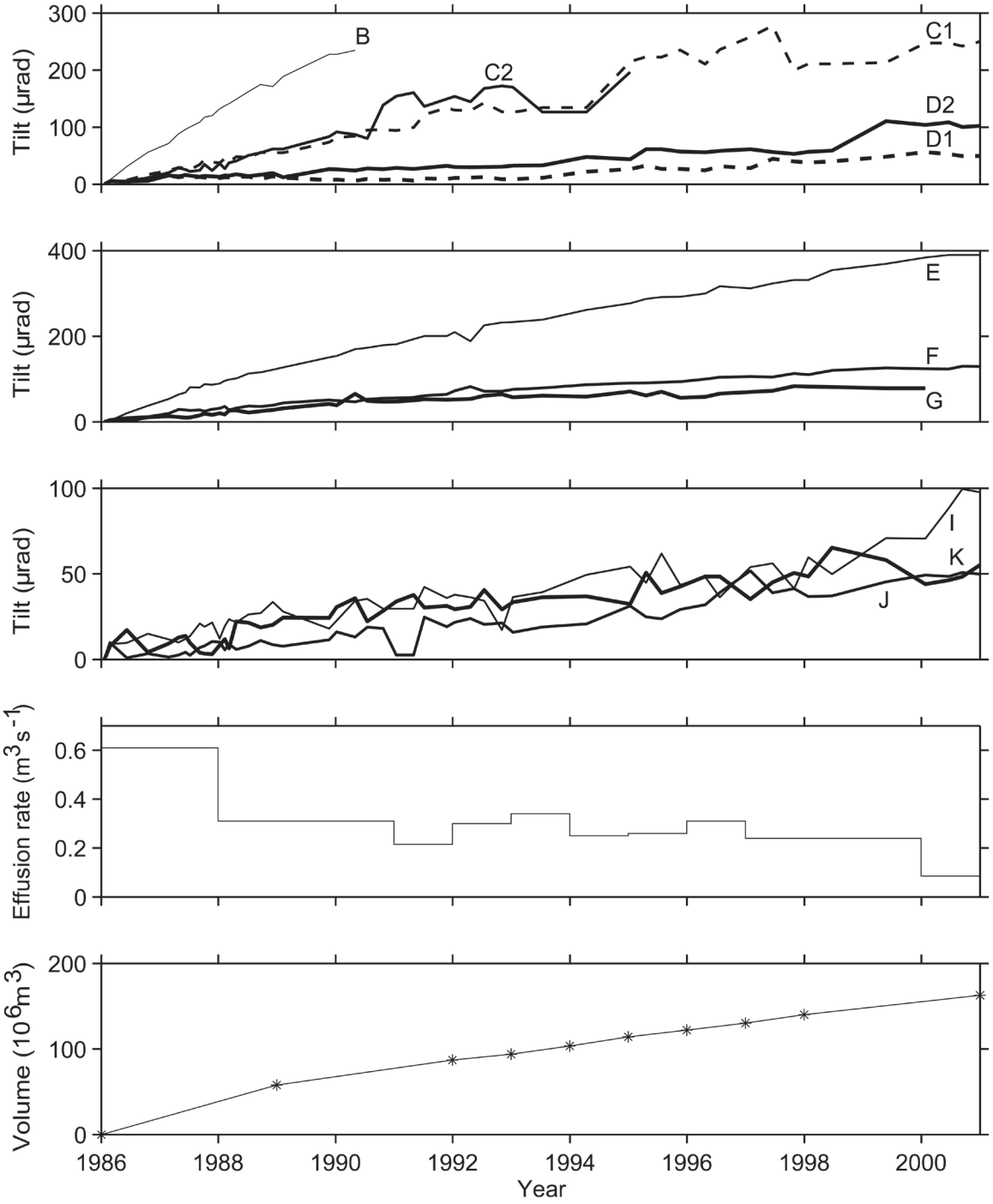

Mauricio M. Mora - Figure 4 - Figure 4.ai

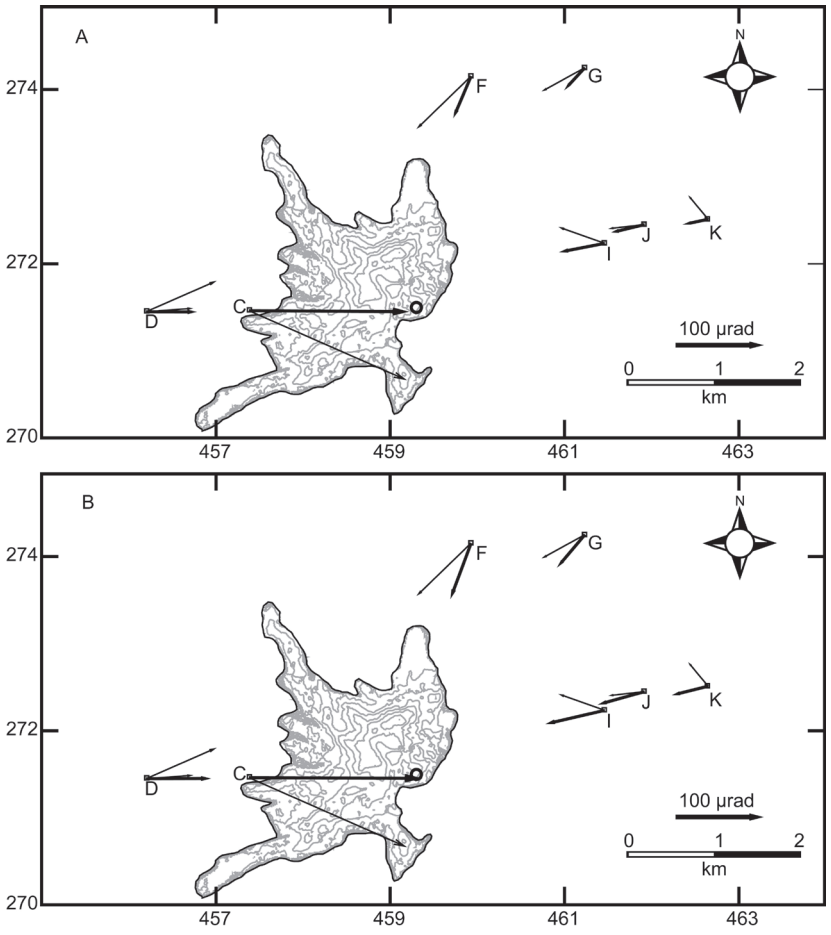

Mauricio M. Mora - Figure 5 - Figure 5.ai

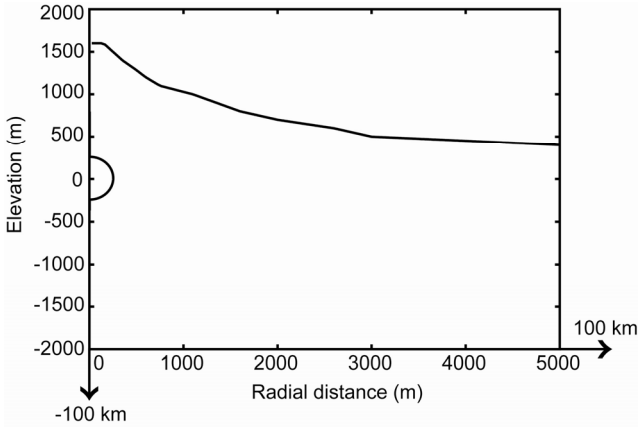

Mauricio M. Mora - Figure 6 - Figure 6.ai